



ELSEVIER

Contents lists available at ScienceDirect

Applied Surface Science

journal homepage: www.elsevier.com/locate/apsusc

Full Length Article

HCOOH dissociation over the core-shell M@Pd bimetallic catalysts: Probe into the effect of the core metal type on the catalytic performance

Min Yang^a, Baojun Wang^a, Zhiqin Li^b, Lixia Ling^a, Riguang Zhang^{a,*}^a Key Laboratory of Coal Science and Technology of Ministry of Education and Shanxi Province, Taiyuan University of Technology, Taiyuan 030024, Shanxi, PR China^b College of Chemistry and Chemical Engineering, Xi'an Shiyou University, Xi'an 710065, Shaanxi, PR China

ARTICLE INFO

Keywords:

HCOOH dissociation
Bimetallic catalyst
Core-shell
Core metal
Catalytic performance

ABSTRACT

The core-shell bimetallic catalysts have exhibited unique catalytic performance due to the bimetallic synergetic effect. In this work, the catalytic activity and selectivity of HCOOH dissociation on the M_{core}@Pd_{shell} (M = Cu, Au, Co, Ni, Ag, Al) catalysts are investigated to reveal the effect of the core metal on the shell Pd catalytic performance. Density functional theory calculations with microkinetic modeling are used. The results showed that compared to the Pd catalyst, M@Pd (M = Au, Co, Ni, Ag) catalysts are highly selective to CO₂ formation, while Al@Pd is favorable for CO formation. Especially, Ag@Pd catalyst not only presents the best activity and selectivity toward CO₂ generation, but also decreases CO adsorption ability to inhibit its poisoning and reduce noble Pd usage. The analysis of the electronic properties about the average Bader charge and *d*-band center corresponding to the shell Pd identify the function of the core metal type in adjusting the shell Pd catalytic performance toward HCOOH dissociation, in which the ligand effect caused by charge transfer between the core metal to the shell Pd plays a key role. This study provides valuable information for the improved performance of the core-shell bimetallic catalysts by altering the types of core metal.

1. Introduction

In recent years, formic acid (HCOOH) has been paid extensive attentions based on its wide range of sources, high mass density, and its weight and volume hydrogen capacity [1–6]. The dissociation of HCOOH can produce CO₂ and H₂ at room temperature, and hydrogen is used as energy source. At present, there are two common mechanisms for HCOOH dissociation, one is a direct path and the other is an indirect path [7–10]. The direct pathway occurs *via* the O–H scission of HCOOH to form HCOO_{ad} intermediate, followed by its C–H scission to form CO₂. In contrast, the indirect pathway produces CO *via* COOH_{ad} intermediate, which may poison the catalyst; alternatively, the dehydrogenation of COOH_{ad} intermediate can also produce CO₂. Further, HCOOH dissociation also occur *via* HCO intermediate [11–13], namely, HCOOH break the C–OH bond to form HCO, and then the C–H bond scission of HCO to produce toxic CO. Therefore, in order to realize HCOOH dissociation to produce hydrogen source at room temperature, it is necessary to develop the catalyst with high selectivity and activity toward CO₂ formation, namely, inhibiting CO formation.

Palladium (Pd) is considered to be the most active monometallic element in HCOOH dissociation [14,15]. However, the catalytic performance of pure Pd catalysts is prone to degradation due to the toxic

effects of CO [16,17]. In order to improve the anti-CO poisoning performance of Pd catalyst and decrease the usage amount of precious metal Pd, the incorporation of the second non-noble metal into Pd catalyst is an applicable approach to increase the catalytic activity of Pd and reduce the catalyst cost, such as PdSn [18,19], PdNi [20–22], PdAg [23–25], PdCu [26–28], PdCo [29], and so on. Up to now, extensive studies have also experimentally and theoretically showed that the core-shell bimetallic catalysts exhibit excellent catalytic performance for HCOOH dissociation [28,30,31]. This is closely related to the electronic properties of the metal surfaces induced by the core metal types, which is called as ligand effect [30,31], in which the charge transfer occur between the core and the shell, the electronic properties of shell surface is optimized. Such as, Tedsree and his colleagues [32] found that the hydrogen production rate in HCOOH dissociation over the Ag@Pd core-shell catalysts was higher by 5 times than that of its corresponding alloy catalysts, which is attributed to the ligand effect caused by charge transfer from the core Ag to the shell Pd. For the pure Pd and Au, the Pd-Au random mixing to form the alloy and core-shell catalysts, the Pd@Au catalysts present the best catalytic activity and selectivity toward CO₂ generation in HCOOH dissociation [33,34], however, it is not clear whether it is also caused by the electronic effect. Mori et al. [35] showed that CO₂ hydrogenation to HCOOH has good

* Corresponding author.

E-mail address: zhangriguang@tyut.edu.cn (R. Zhang).<https://doi.org/10.1016/j.apsusc.2019.144938>

Received 29 August 2019; Received in revised form 12 November 2019; Accepted 3 December 2019

Available online 05 December 2019

0169-4332/ © 2019 Elsevier B.V. All rights reserved.

selectivity due to the electronic effect caused by Ag atom on the Pd@Ag/TiO₂ catalyst, and its activity is higher than that of Pd/TiO₂ catalyst. However, up to now, a fundamental understanding the effect of the core metal incorporation in the core-shell M@Pd bimetallic catalysts on the catalytic performance of the shell Pd toward HCOOH dissociation were still unclear, as a result, a general information about the design clue of the core-shell M@Pd bimetallic catalysts for the selectivity and activity improvement of HCOOH dissociation to product H₂ and CO₂ cannot be provided.

In this work, aiming at identifying the effect of core metal type on the shell Pd catalytic activity and selectivity in HCOOH dissociation, the possible mechanism of HCOOH dissociation over a series of M_{core}@Pd_{shell} (M = Cu, Au, Co, Ni, Ag, Al) bimetallic catalysts have been fully investigated utilizing the combination of density functional theory (DFT) calculations with microkinetic modeling. Then, the Pd catalyst was used as a reference, the catalytic activity and selectivity of HCOOH dissociation on the M_{core}@Pd_{shell} catalysts were evaluated to obtain the effect of core metal type on the shell Pd catalytic performance. The results are expected to provide a valuable clue for designing efficient, low-cost core-shell Pd-based bimetallic catalysts in HCOOH dissociation.

2. Computational details

2.1. Computational method

All calculations were performed based on the Vienna ab initio simulation package (VASP) [36–38]. The projector augmented wave (PAW) pseudopotentials were used to calculate the interaction between the core ions and the valence electrons [39]. The correlation potentials of ion-electron exchange were approximated by the generalized gradient approximation of GGA and PBE (Perdew-Burke-Ernzerhof) functions [40–42]. The cut-off energy of plane wave basis was 400 eV and a (3 × 3 × 1) *k*-point grid was established by using Monkhorst-Pack method [43]. The convergence results were obtained when the total energy change between two continuous steps is less than 1 × 10⁻⁵ eV and the force constant is less than 0.03 eV Å, respectively. Spin polarization was considered. The combination of the climbing-image nudged elastic band (CI-NEB) [44,45] and dimer methods [46,47] was used to search the transition states (TS). Frequency analysis was performed to verify the transition state structure corresponding to only one imaginary frequency. Further, HCOOH dissociation typically occurs under the room temperature (298 K) [48–51], thus, the energy values including adsorption and reaction were calculated at 298 K in this study (see details in the Part 1 of Supplementary Material).

2.2. Computational model

It is well-known that the mostly exposed surface of face-centered-cubic (FCC) metal is the (1 1 1) surface, such as the metals Pd, Cu, Au, Ag, Co, Ni and Al [25,52–57], which corresponds to the lattice constants of 3.955, 3.623, 4.078, 4.086, 3.544, 3.523, and 3.992 Å, respectively [58]. Here, three-layer *p*(3 × 3) Pd(1 1 1), Cu(1 1 1), Au(1 1 1), Ag(1 1 1), Co(1 1 1), Ni(1 1 1) and Al(1 1 1) surfaces are constructed to simulate the Pd, Cu, Au, Ag, Co, Ni and Al catalysts. A 15 Å vacuum gap is set to avoid the slab interaction in the *z* direction. For the core-shell M@Pd (M = Cu, Au, Co, Ni, Ag, Al) bimetallic catalysts, they are modeled by replacing the monolayer surface M atoms of M(1 1 1) (M = Cu, Au, Co, Ni, Ag, Al) surface with the Pd atoms, respectively. Further, the top two layers together with the adsorbed species are relaxed, and the bottom layer is fixed during the calculations. The optimized structures of the pure Pd and M_{core}@Pd_{shell} (M = Cu, Au, Co, Ni, Ag, Al) catalysts are presented in Fig. 1.

3. Results and discussion

The dissociation of HCOOH starts from its adsorption of gaseous form onto the catalyst surface; subsequently, it generates different intermediates by activating the C–H, O–H and C–OH bonds. On the basis of previous studies [7–13], four possible paths can be obtained for HCOOH dissociation, as shown in Scheme 1, Paths 1 and 2 go through the corresponding HCOO and COOH intermediates to produce CO₂; Path 3 goes through the COOH intermediate to produce CO; Path 4 is the C–OH bond scission of HCOOH to generate the HCO intermediate, followed CO generation through the C–H bond scission of HCO.

The adsorption of all species involved in the four paths of HCOOH dissociation are firstly examined on the pure Pd and core-shell Cu@Pd, Au@Pd, Co@Pd, Ni@Pd, Ag@Pd, Al@Pd catalysts. Fig. S1 and Table S1 present the most stable configurations of all adsorbed species, the key geometric parameters and adsorption free energies.

3.1. HCOOH dissociation over the Pd and M_{core}@Pd_{shell} catalysts

3.1.1. Formation of CO₂

For the Path 1, see Figs. 2–8, firstly, *trans*-HCOOH absorbed at the top Pd site goes through the O–H bond scission *via* the transition state TS_{x-1} (x = 1–7) to produce the HCOO and H species, where the *bi*-HCOO binds to the Pd-Pd bridge sites, and H is located at the near fcc site. This step have the corresponding activation barriers of 50.6, 55.2, 39.9, 57.0, 65.7, 32.8 and 68.3 kJ·mol⁻¹ on the pure Pd and core-shell Cu@Pd, Au@Pd, Co@Pd, Ni@Pd, Ag@Pd, Al@Pd catalysts, respectively. Previous DFT studies [59] also showed that this step over the Au-decorated Pd catalysts corresponds to the activation barrier of about 44 kJ·mol⁻¹. Meanwhile, this reaction is endothermic by 18.8, 44.9 and 37.8 kJ·mol⁻¹ on the Cu@Pd, Co@Pd and Ni@Pd catalysts, while those are exothermic by 1.2, 17.7, 27.5 and 35.7 kJ·mol⁻¹ on the Pd, Au@Pd, Ag@Pd and Al@Pd catalysts, respectively, which is attributed to the stronger adsorption ability of *bi*-HCOO on these catalysts. Then, the *bi*-HCOO species can isomerize to form *mono*-HCOO *via* the transition state TS_{x-2} (x = 1–7), which facilitates the placement of H atoms and the cleavage of C–H bond; it is found that *bi*-HCOO takes a high activation barrier to form metastable *mono*-HCOO intermediate, they are 92.8, 78.0, 77.7, 78.6, 77.5, 61.4 and 89.2 kJ·mol⁻¹ on the Pd and M@Pd (M = Cu, Au, Co, Ni, Ag, Al) catalysts. This step is disadvantageous in dynamics, which is similar to our previous work on PtAu catalysts [60]. This explains why only surface HCOO intermediates were observed on Pd and Pt catalyst [61,62]. Further, *mono*-HCOO *via* the transition state TS_{x-3} (x = 1–7) breaks the C–H bond to easily produce the H and CO₂, where CO₂ leaves the catalyst surface to become gas phase; the corresponding activation barriers are 7.9, 4.9, 5.5, 0.7, 1.8, 6.2 and 29.4 kJ·mol⁻¹ on the pure Pd and core-shell Cu@Pd, Au@Pd, Co@Pd, Ni@Pd, Ag@Pd, Al@Pd catalysts, respectively; and it is a strong exothermic reaction. For *mono*-HCOO → CO₂ + H, extensive DFT calculations [45,59,60] also showed that this step is advantageous in kinetics with the activation barrier of about 10 kJ·mol⁻¹ on the Pd, PtAu and PdCu catalysts. From the above analysis, it can be concluded that the activation barrier of *trans*-HCOOH → HCOO + H and HCOO → CO₂ + H on the Ag@Pd catalyst can be reduced in comparison with the Pd catalyst; namely, the core-shell Ag@Pd catalyst presents better activity of HCOOH dissociation to produce CO₂ *via* the HCOO intermediate.

In Path 2, *trans*-HCOOH firstly rotate the H–C–O bond *via* the transition state TS_{x-4} (x = 1–7) to convert into *cis*-HCOOH, as a result, the C–H bond of *cis*-HCOOH towards the catalysts surface is beneficial for its cleavage. The corresponding activation barriers are 70.8, 59.6, 68.2, 58.4, 54.3, 67.5 and 60.9 kJ·mol⁻¹ on the pure Pd and core-shell Cu@Pd, Au@Pd, Co@Pd, Ni@Pd, Ag@Pd, Al@Pd catalysts, respectively. These reactions are endothermic by 25.7, 14.8, 30.3, 22.6, 20.0, 10.6 and 11.7 kJ·mol⁻¹. For the conversion of the *trans*-HCOOH → *cis*-HCOOH, this is consistent with the previous calculation by Duan et al.

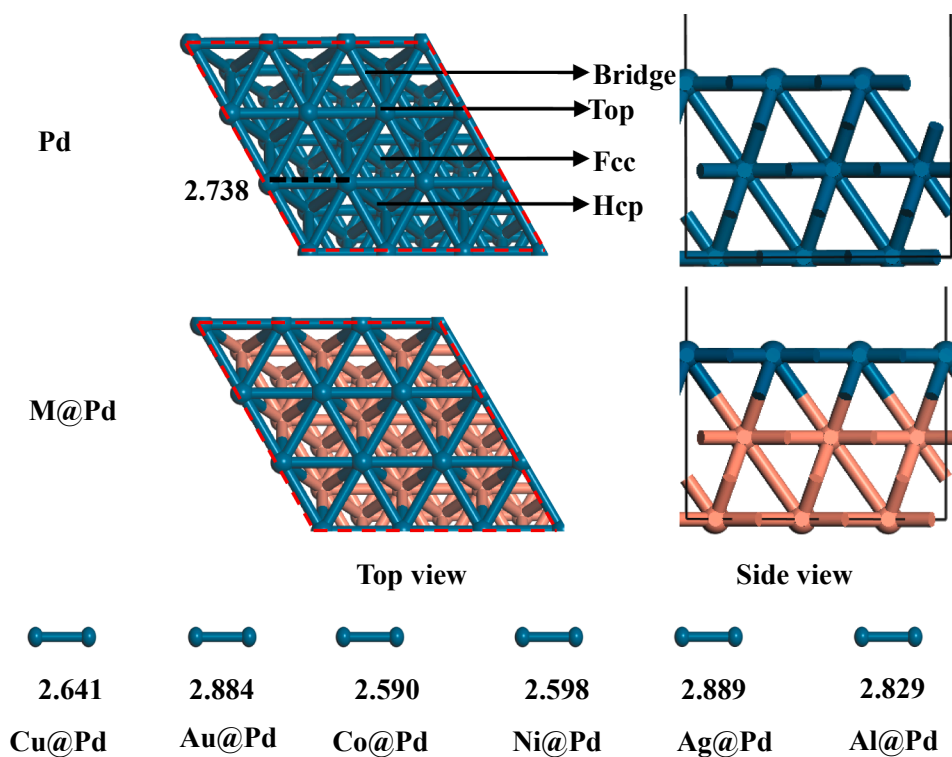
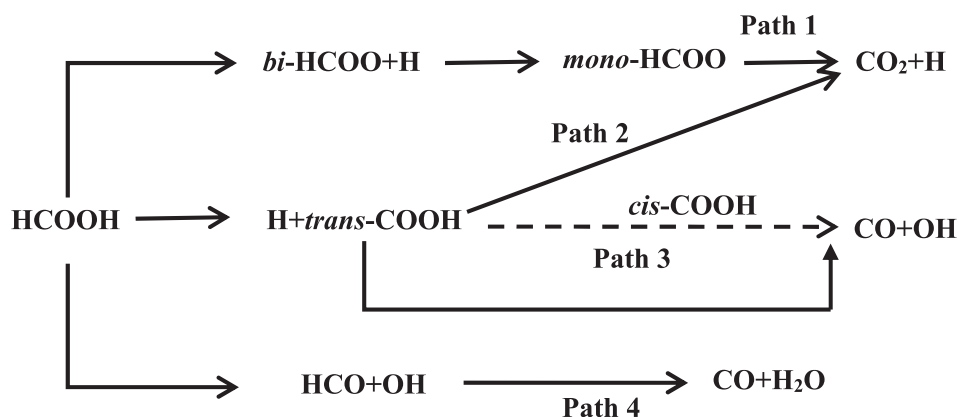


Fig. 1. Side and top views of the optimized configurations of Pd and M@Pd (M = Cu, Au, Co, Ni, Ag, Al) catalysts together with the corresponding adsorption sites and surface Pd-Pd bond length. (Bond length: Å).



Scheme 1. Proposed reaction mechanism of HCOOH dissociation over the Pd, Cu@Pd, Au@Pd, Co@Pd, Ni@Pd, Ag@Pd and Al@Pd catalysts.

[60]. Subsequently, the C–H bond scission of *cis*-HCOOH can produce the COOH and H through the transition state TSx-5(x = 1–7), where the adsorbed *trans*-COOH binds to the top Pd sites, H is adsorbed at the near fcc site. The corresponding activation barriers are 31.5, 50.8, 24.3, 67.7, 56.5, 32.2 and 67.4 kJ·mol⁻¹, respectively; these reactions are endothermic by 14.0, 0.8 and 39.1 kJ·mol⁻¹ on the M@Pd (M = Co, Ni, Al) catalysts, those are exothermic by 57.3, 32.2, 71.4 and 68.1 kJ·mol⁻¹ on the Pd, Cu@Pd, Au@Pd and Ag@Pd catalysts, respectively, which is attributed to that the *trans*-COOH has a higher adsorption ability on these catalysts; this agrees with the calculated results by Yuan and co-workers [59] on PdAu catalyst with different Pd/Au proportions. Finally, *trans*-COOH breaks the C–H bond to produce CO₂ and H via the transition state TSx-6(x = 1–7), in which CO₂ is far away from the catalyst surfaces. The corresponding activation barriers are 60.1, 57.7, 51.0, 61.5, 64.0, 46.7 and 95.5 kJ·mol⁻¹ over the seven catalysts, and they are all strong exothermic reactions. Based on above analysis, compared to the Pd catalyst, the activation barrier of *trans*-HCOOH → COOH + H and COOH → CO₂ + H reactions on the Ag@Pd catalyst can be reduced or comparable in kinetics; namely, HCOOH dissociation over the core-shell Ag@Pd catalyst still has better

catalytic activity toward CO₂ formation in the path of COOH intermediate. In addition, the C–H bond scission of *cis*-COOH leading to CO₂ and H is also considered; our calculated results found that *cis*-COOH isomerization to *trans*-COOH must be firstly needed instead of its C–H bond cleavage.

3.1.2. Formation of CO

Path 3 also begins with the co-adsorption of *trans*-COOH and H. The formation of CO comes from two ways via the *trans*- and *cis*-COOH intermediates. The co-adsorbed CO and OH species are directly formed through the C–O bond scission of *trans*-COOH via the transition state TSx-7(x = 1–7), generally CO fall at the hollow sites; the corresponding activation barriers are 79.1, 127.7, 75.1, 94.5, 94.4, 83.4 and 53.7 kJ·mol⁻¹ on the pure Pd and core-shell Cu@Pd, Au@Pd, Co@Pd, Ni@Pd, Ag@Pd, Al@Pd catalysts, in which the Al@Pd catalyst is favorable for CO formation compared to the pure Pd catalyst. As for *cis*-COOH, it comes from the *trans*-COOH by rotating the O–H bond via the transition state TSx-8(x = 1–7) with the corresponding activation barriers of 51.3, 48.6, 44.6, 47.2, 42.8, 51.1 and 53.7 kJ·mol⁻¹ over the seven catalysts, subsequently, the formation of CO via the transition

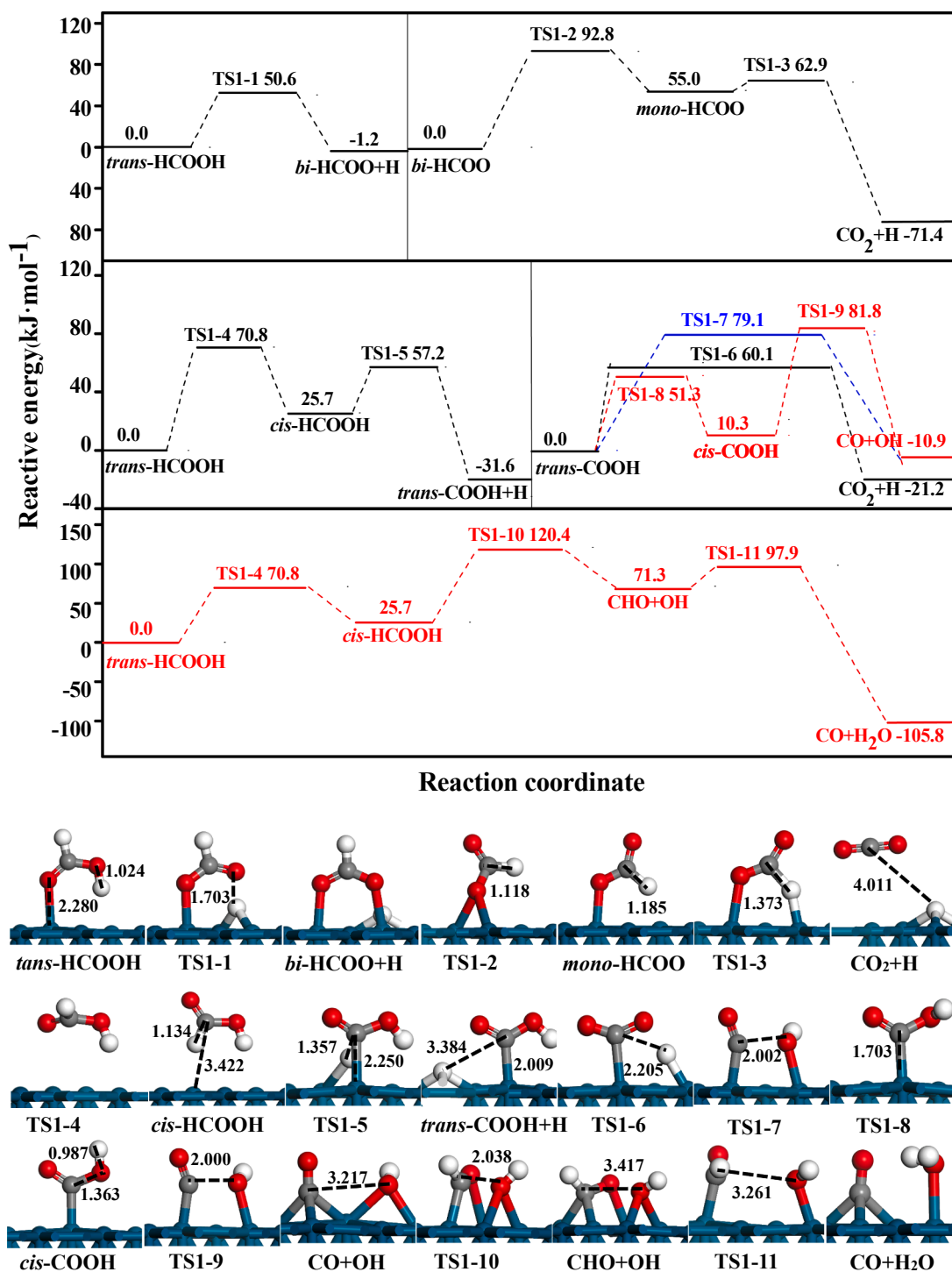


Fig. 2. Potential energy profiles of HCOOH dissociation via the pathways of HCOO, COOH and CHO intermediates with the initial states, transition states (TSs) and final states over the pure Pd catalyst. Bond length is in Å.

state TS_x-9 (x = 1–7) are 71.5, 71.3, 62.5, 81.5, 88.8, 72.4 and 47.9 kJ·mol⁻¹ over the seven catalysts, in which the Al@Pd catalyst is still favorable for CO formation in comparison with the Pd catalyst. These results show that irrespective of *trans*- and *cis*-COOH species, the Al@Pd catalyst is in favor of its C–OH bond scission to produce CO among seven types of catalysts. Meanwhile, CO formation from *cis*-COOH was easier than that from *trans*-COOH, the origin is attribute to the orientation of the O–H bond, in which the O–H bonds of *trans*-COOH need to be rotated, whereas the O–H bond rotation of *cis*-COOH is required. This is the reason why *cis*-COOH intermediate was

considered in many calculations [48,60].

In Path 4, CO formation is via the HCO intermediate. As shown in Figs. 2–8, Firstly, *trans*-HCOOH needs to overcome a barrier via the transition state TS_x-4 (x = 1–7) to convert into *cis*-HCOOH, then, *cis*-HCOOH breaks the C–OH bond to form HCO intermediate via the transition state TS_x-10 (x = 1–6), the corresponding activation barriers are 94.7, 160.1, 122.4, 139.7, 135.8, 112.5 and 290.5 kJ·mol⁻¹ on the pure Pd and core-shell Cu@Pd, Au@Pd, Co@Pd, Ni@Pd, Ag@Pd, Al@Pd catalysts, respectively, suggesting that the core-shell Cu@Pd, Au@Pd, Co@Pd, Ni@Pd, Ag@Pd, Al@Pd catalysts are kinetically

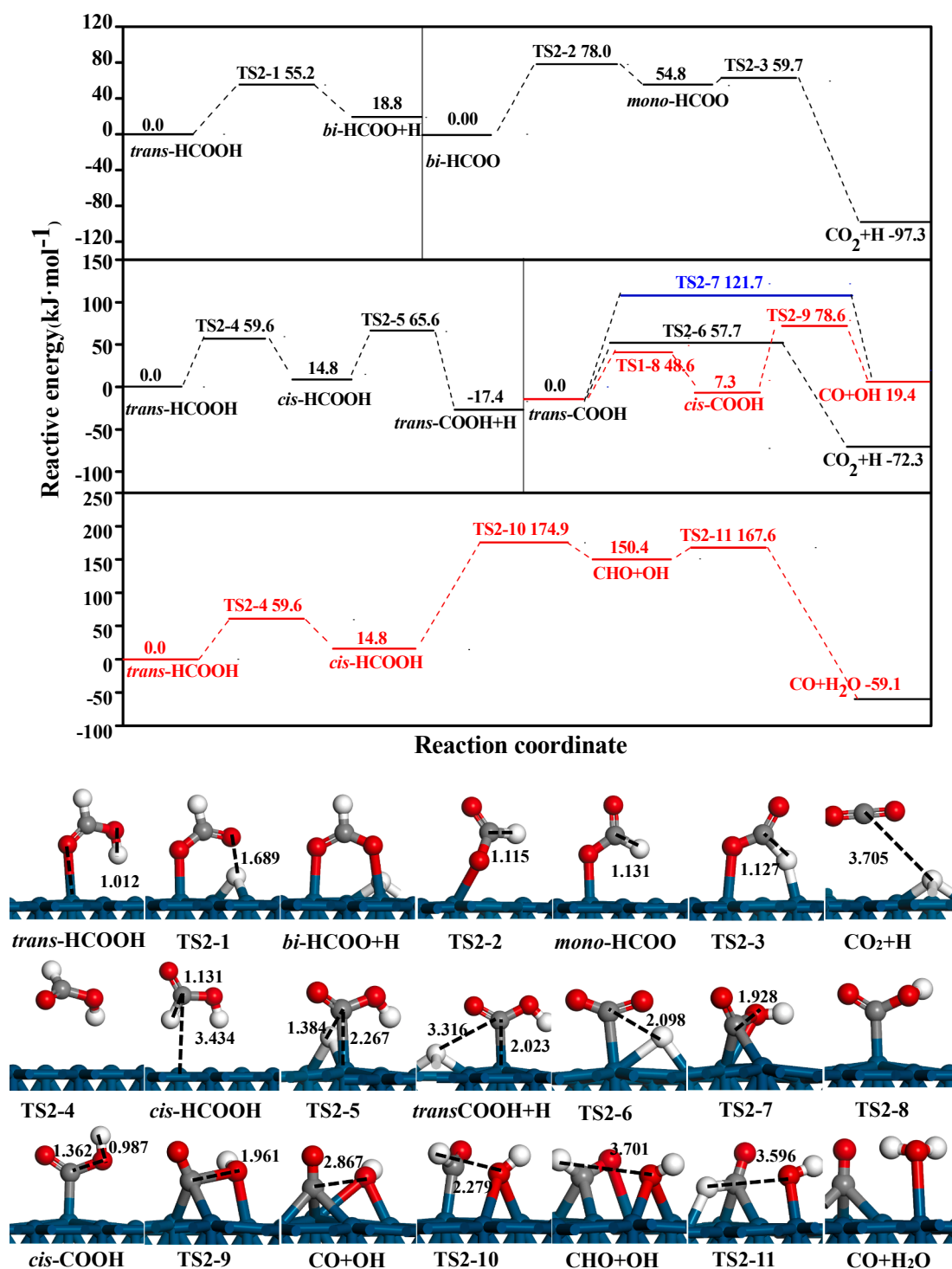


Fig. 3. Potential energy profiles of HCOOH dissociation via the pathways of HCOO, COOH and CHO intermediates with the initial states, transition states (TSs) and final states over the Cu@Pd catalyst. Bond length is in Å.

unfavorable for the C–OH bond scission of HCOOH to produce HCO intermediate than the pure Pd catalyst, subsequently, the co-adsorbed HCO and OH species to produce CO and H_2O species via the transition state TSx-11 ($x = 1-7$) have the lower activation barriers of 26.6, 17.2, 14.8, 18.1, 11.4, 19.3 and $34.5 \text{ kJ}\cdot\text{mol}^{-1}$ over the seven catalysts; meanwhile, this reaction is highly exothermic. Thus, the C–OH bond scission of HCOOH is much difficult in kinetics compared to the O–H and C–H bond breakage, CO formation through the HCO intermediate is kinetically unfavorable compared to that through the COOH intermediate.

3.2. The optimal path and dominant products of HCOOH dissociation

Above results show that CO prefers to be produced via the COOH intermediate instead of the HCO intermediate on the pure Pd and core-shell Cu@Pd, Au@Pd, Co@Pd, Ni@Pd, Ag@Pd, Al@Pd catalysts; namely, the path via HCO intermediates can be excluded, which is consistent with the research on the Pt and PtAg catalysts, and so on [63–65]. However, CO_2 formation mainly goes through the COOH or HCOO intermediate, which depends on the types of core metal.

On the Pd, Cu@Pd and Au@Pd catalysts, as shown in Figs. 2–4, the

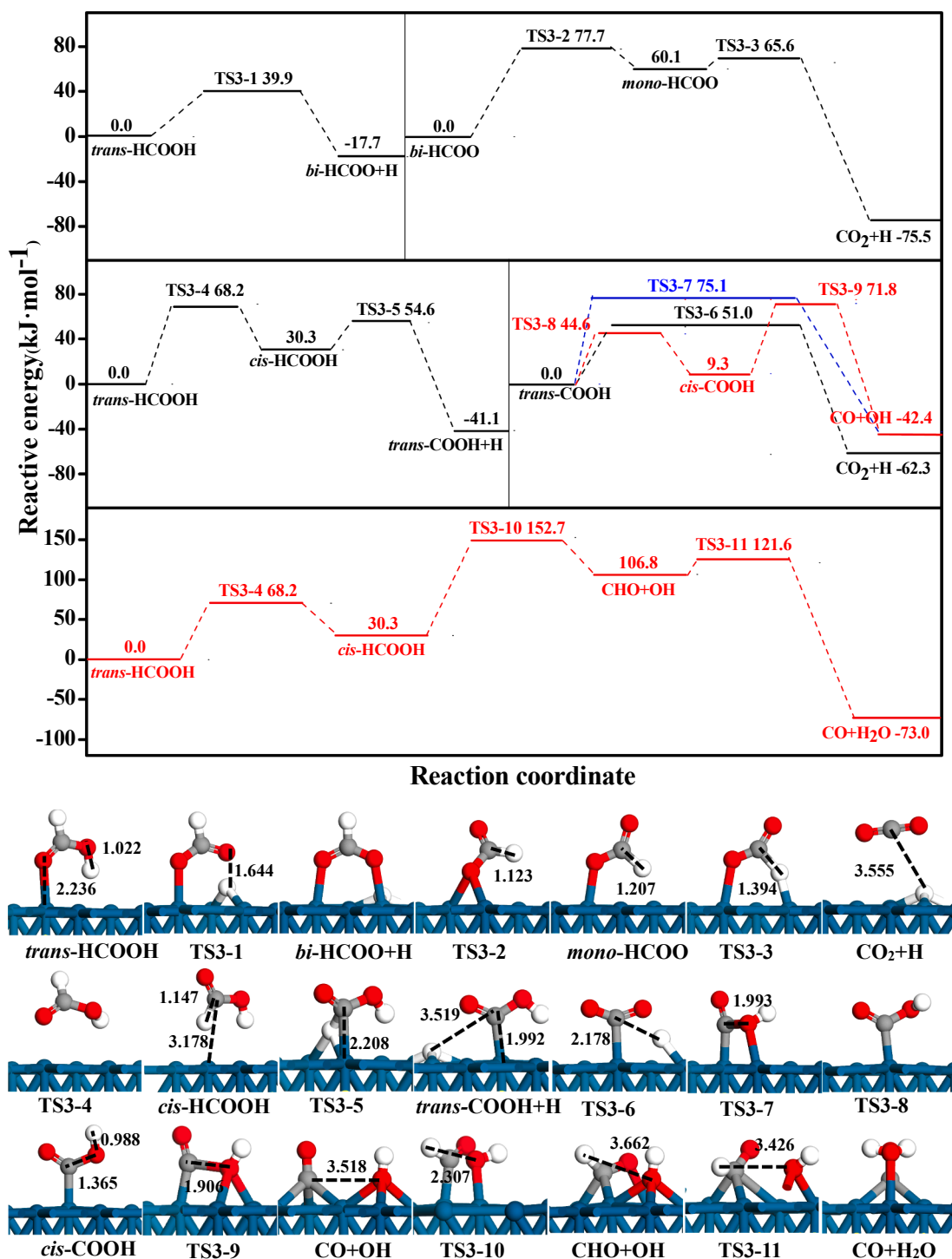


Fig. 4. Potential energy profiles of HCOOH dissociation via the pathways of HCOO, COOH and CHO intermediates with the initial states, transition states (TSs) and final states over the Au@Pd catalyst. Bond length is in Å.

generation of CO₂ mainly goes through COOH intermediates rather than HCOO intermediates, the rate-controlled step is *trans*-HCOOH → COOH + H with the corresponding activation barriers of 70.8, 68.2 and 65.6 kJ·mol⁻¹, respectively. The production of CO mainly stems from the COOH intermediates. Starting from the COOH intermediate, CO₂ generation is kinetically favorable than CO formation over the Pd (60.1 vs. 79.1 kJ·mol⁻¹), Cu@Pd (57.7 vs. 78.6 kJ·mol⁻¹) and Au@Pd (51.0 vs. 71.8 kJ·mol⁻¹) catalysts. On the Co@Pd catalyst, as shown in Fig. 5, the generation of CO₂ mainly goes through HCOO intermediates rather than COOH intermediates, and the rate-controlled step is *bi*-HCOO →

mono-HCOO with the activation barrier of 78.6 kJ·mol⁻¹. Comparing the rate-controlled step of CO₂ and CO formation, CO₂ formation is still favorable than CO in kinetics (78.6 vs. 91.1 kJ·mol⁻¹). As shown in Figs. 6 and 7, CO₂ generation via the COOH and HCOO intermediates correspond to the activation barriers of 77.5 and 76.5 kJ·mol⁻¹ on the Ni@Pd, and those are 61.4 and 67.5 kJ·mol⁻¹ over the Ag@Pd, respectively; thus, the generation of CO₂ has two parallel path via the COOH and HCOO intermediates. CO generation have the activation barriers of 94.4 and 83.4 kJ·mol⁻¹ on the Ni@Pd and Ag@Pd catalysts, respectively. Thus, the main product obtained from HCOOH

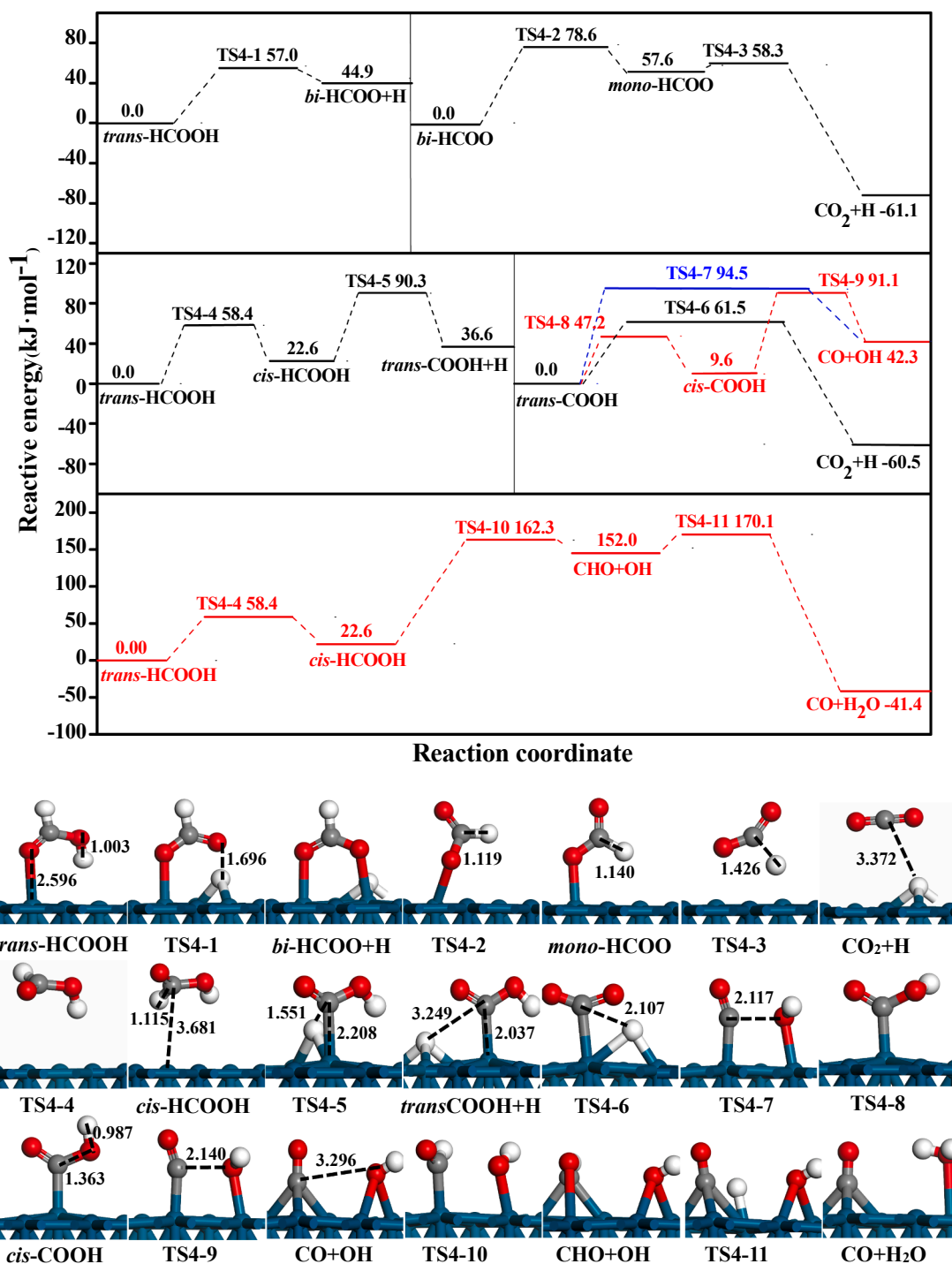


Fig. 5. Potential energy profiles of HCOOH dissociation via the pathways of HCOO, COOH and CHO intermediates with the initial states, transition states (TSs) and final states over the Co@Pd catalyst. Bond length is in Å.

dissociation is CO_2 on the pure Pd and core-shell Cu@Pd, Au@Pd, Co@Pd, Ni@Pd and Ag@Pd catalysts.

As shown in Fig. 8, over the Al@Pd catalyst, the pathway to generate CO_2 via the HCOO and COOH intermediate are also parallel (93.1 vs. 95.5 $\text{kJ}\cdot\text{mol}^{-1}$). The optimal path of CO generation is *trans*-HCOOH dissociation via the COOH intermediate, the rate-controlled step is *trans*-HCOOH \rightarrow COOH + H with the corresponding activation barrier of 79.1 $\text{kJ}\cdot\text{mol}^{-1}$. Thus, the generation of CO is much higher than that of CO_2 in kinetics (79.1 vs. 93.1 $\text{kJ}\cdot\text{mol}^{-1}$), CO becomes the dominant product.

3.3. The effect of catalyst structure properties on the catalytic performance

3.3.1. The effect of core metal type on the product selectivity of COOH dissociation

As mentioned above, the optimal path of CO generation always goes through COOH intermediates over the seven catalysts. Similarly, COOH intermediates also produce the target product CO_2 . Beginning with the *trans*-COOH, CO_2 generation by the O–H bond breaking corresponds to the activation barriers of 60.1, 57.7, 51.0, 61.5, 64.0, 46.7 and 95.5 $\text{kJ}\cdot\text{mol}^{-1}$, respectively; while CO generation by the C–OH bond scission are 79.1, 127.7, 75.1, 94.5, 94.4, 83.4 and 53.7 $\text{kJ}\cdot\text{mol}^{-1}$ on

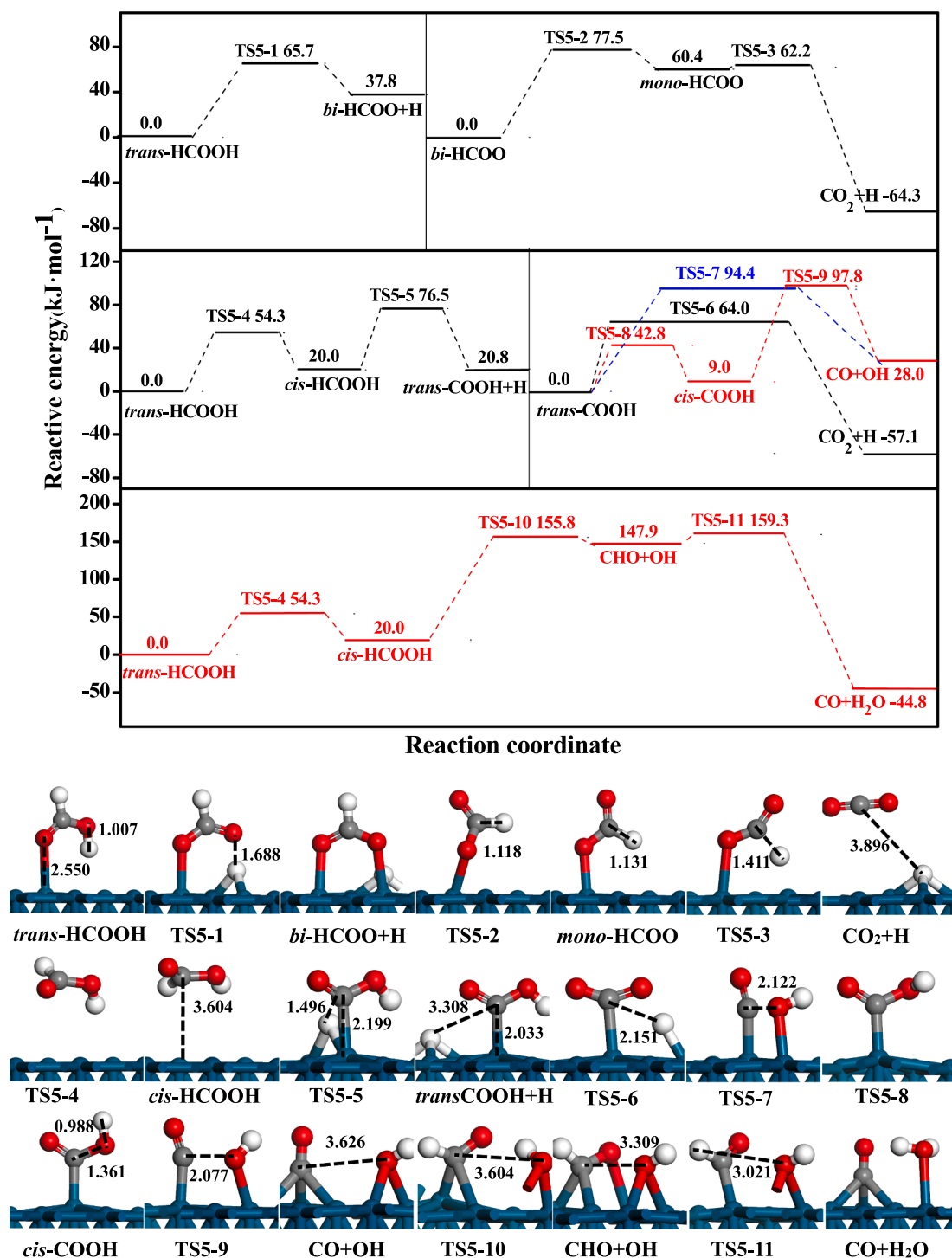


Fig. 6. Potential energy profiles of HCOOH dissociation via the pathways of HCOO, COOH and CHO intermediates with the initial states, transition states (TSs) and final states over the Ni@Pd catalyst. Bond length is in Å.

the pure Pd and core-shell Cu@Pd, Au@Pd, Co@Pd, Ni@Pd, Ag@Pd, Al@Pd catalysts, respectively. It can be seen that the Pd and M@Pd (M = Cu, Au, Co, Ni, Ag) catalysts are beneficial for the formation of CO_2 while the Al@Pd catalyst is advantageous to the formation of CO. Namely, COOH intermediates play a key function in determining the product selectivity of HCOOH dissociation.

To better clarify the effect of the M@Pd catalyst on the product selectivity of COOH dissociation, the difference charge density for the stable adsorption configurations of *trans*-COOH intermediate among the seven catalysts are presented, as shown in Fig. 9, which indicates that

the charge of COOH intermediates accumulates at the region of the Pd-C and C-OH bonds over the Al@Pd catalyst, while the region of O-H bond has no charge-rich, namely, there is strong charge transfer between C and OH, which enhances the dissociation activity of COOH via the C-OH bond cleavage to generate CO. On the contrary, the charge of COOH intermediates accumulates at the region of the Pd-C and O-H bonds, and the H-oriented surface has a large electron cloud on the pure Pd and core-shell Cu@Pd, Au@Pd, Co@Pd, Ni@Pd, Ag@Pd catalysts, which makes the cleavage of the O-H bond easier to form CO_2 instead of the C-OH bond scission leading to CO.

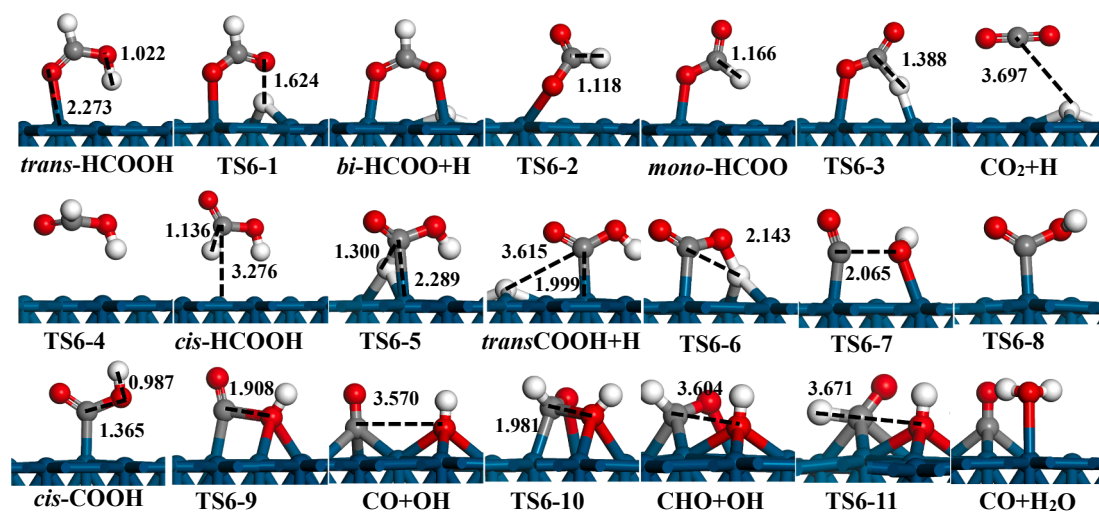
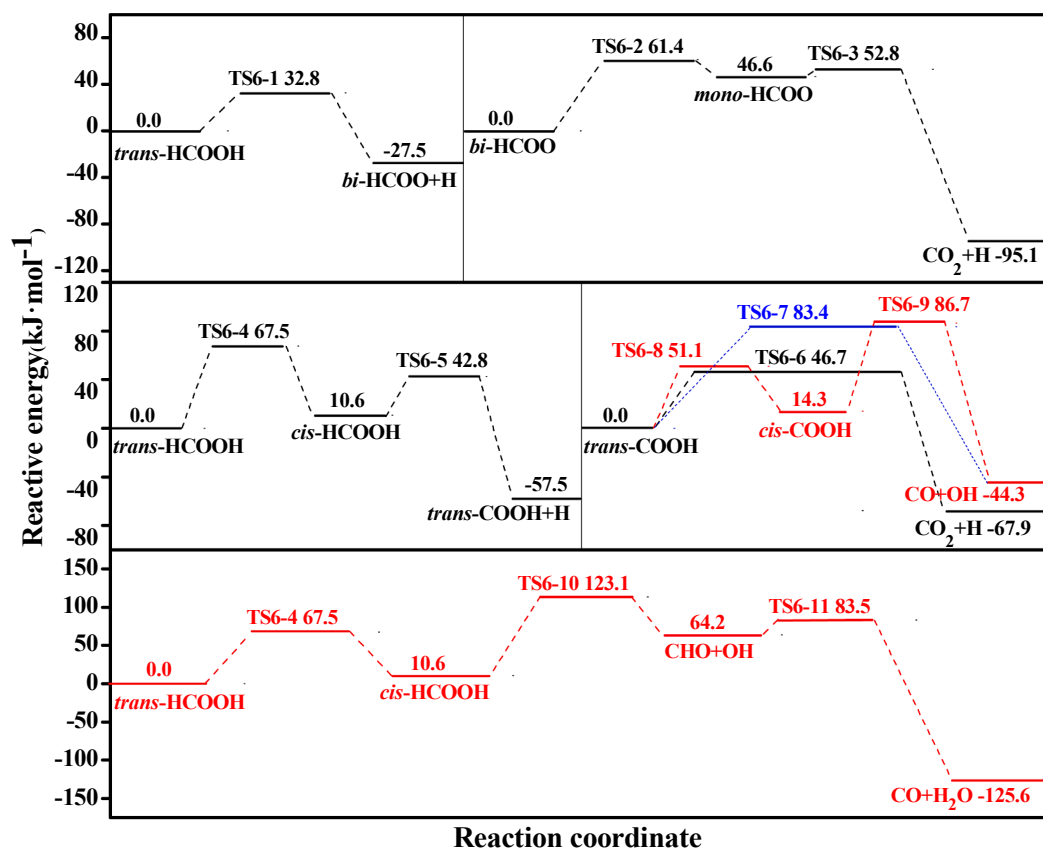


Fig. 7. Potential energy profiles of HCOOH dissociation via the pathways of HCOO, COOH and CHO intermediates with the initial states, transition states (TSs) and final states over the Ag@Pd catalyst. Bond length is in Å.

3.3.2. The effect of core metal type on the catalytic performance

To better understand the effect of the core metal type on the activity and selectivity toward HCOOH dissociation, the activation barriers of the rate-controlled steps in the optimal path of CO₂ and CO generation are analyzed. As shown in Fig. 10, the activation barriers of CO₂ formation are 70.8, 65.6, 68.2, 78.6, 76.5, 61.4 and 79.1 kJ·mol⁻¹ on the pure Pd and core-shell Cu@Pd, Au@Pd, Co@Pd, Ni@Pd, Ag@Pd, Al@Pd catalysts, thus, the activity of CO₂ formation follow the order of: Ag@Pd > Cu@Pd > Au@Pd > Pd > Ni@Pd > Co@Pd > Al@Pd, namely, compared to the pure Pd catalyst, Cu@Pd, Au@Pd and Ag@Pd catalysts can improve the activity of HCOOH dissociation, whereas the Ni@Pd, Co@Pd and Al@Pd catalysts cannot do the same performance.

On the other hand, the difference of activation barrier between the generations of CO₂ and CO was calculated to evaluate the selectivity of CO₂ formation. The more negative difference means the higher CO₂ selectivity. The energy differences between CO₂ and CO are -8.3, -13.0, -3.6, -12.5, -17.9, -22.0 and 14.0 kJ·mol⁻¹ on the pure Pd and core-shell Cu@Pd, Au@Pd, Co@Pd, Ni@Pd, Ag@Pd, Al@Pd catalysts. The order of CO₂ selectivity is that: Ag@Pd > Ni@Pd > Co@Pd > Cu@Pd > Pd > Au@Pd > Al@Pd, indicating that both Ag@Pd and Ni@Pd catalysts exhibit the highest selectivity toward CO₂ formation. Further, the relative selectivity of CO₂ generation was calculated using microkinetic modeling, the selectivity of CO₂ can reach nearly 99.99% on the Au@Pd, Ag@Pd, Co@Pd and Ni@Pd catalysts;

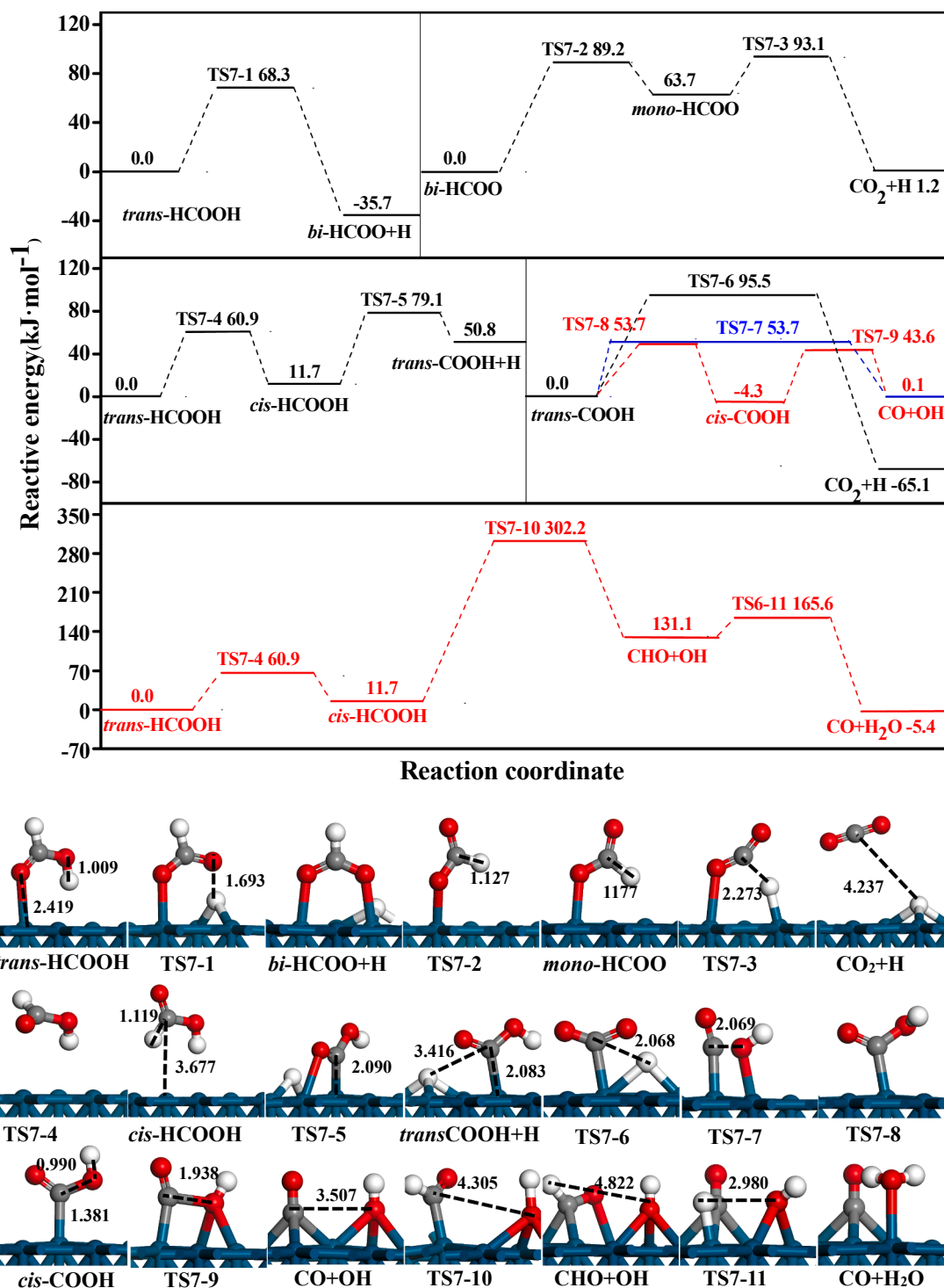


Fig. 8. Potential energy profiles for HCOOH dissociation via the pathways of HCOO, COOH and CHO intermediates with the initial states, transition states (TSs) and final states over the Al@Pd catalyst. Bond length is in Å.

both Pd and Cu@Pd catalysts can reach 99.01% and 85.87%, respectively, while that of Al@Pd catalyst is only 4.77%.

Based on the above analysis, considering the activity and selectivity of CO₂, among the M@Pd catalysts, the core-shell Ag@Pd catalyst not only enhance CO₂ selectivity and its formation activity, but also reduces CO adsorption capacity and increase the resistance ability toward CO. Further, for the Ag@Pd catalyst, the non-noble metal Ag incorporation as the core can reduce the usage amount of precious metal Pd, and therefore decrease the cost of the catalyst.

3.3.3. The analysis of electronic properties for the Pd and M@Pd catalysts

Based on above results, the surface electronic properties of these catalysts were further analyzed to illustrate the effect of core metal on the selectivity and activity of HCOOH dissociation. The average charge polarization ($\Delta\sigma$) of surface Pd atoms on the pure Pd and core-shell Cu@Pd, Au@Pd, Co@Pd, Ni@Pd, Ag@Pd, Al@Pd catalysts are obtained by the Bader charge and the corresponding values are 0.006, -0.130, -0.022, -0.125, -0.106, -0.088 and -0.875 e, respectively. Meanwhile, the corresponding activation barriers of CO₂

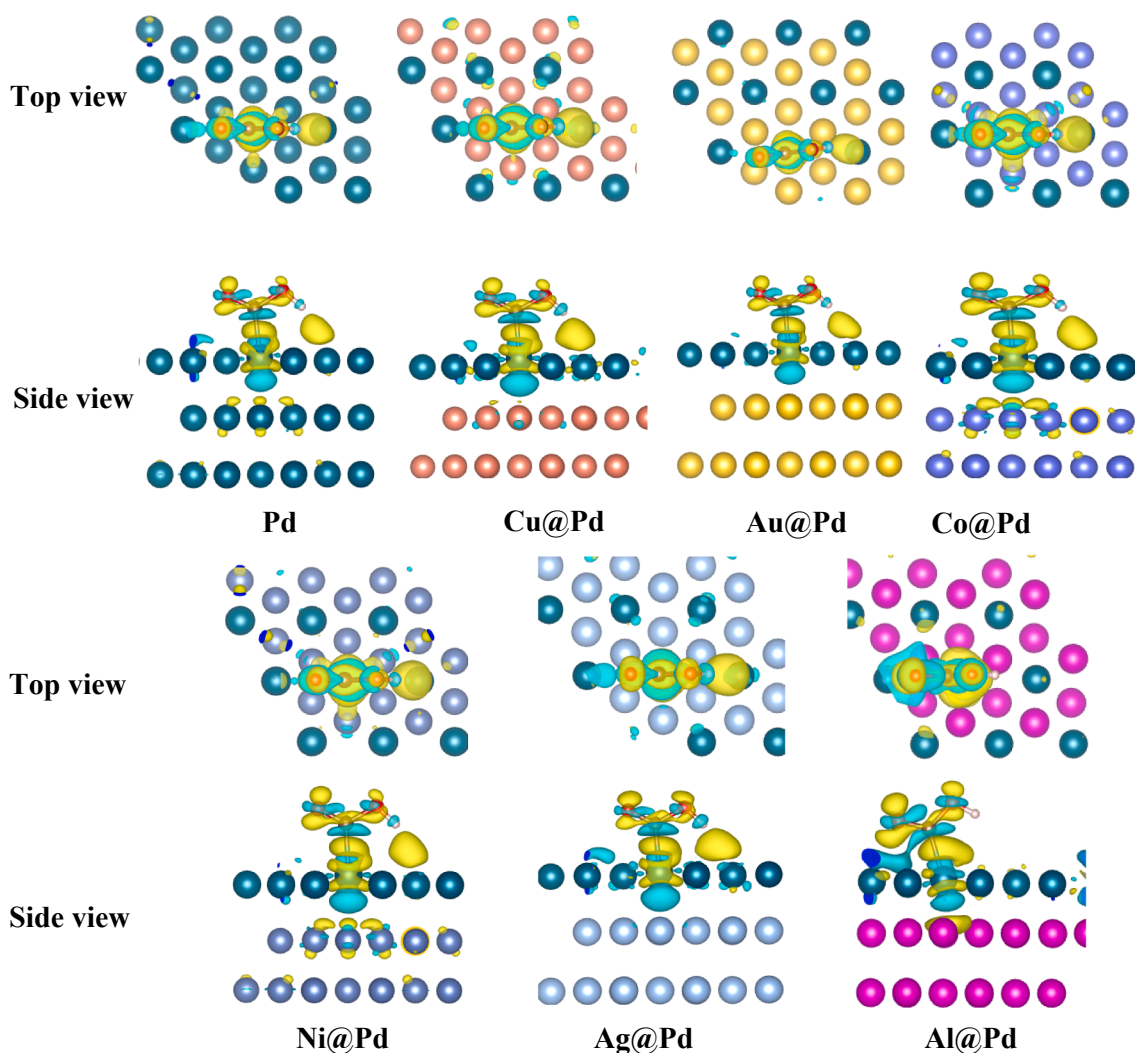


Fig. 9. The charge redistribution with the difference charge density $\Delta\rho = \rho_{\text{COOH}/\text{M}} - \rho_{\text{COOH}/\text{PM}} - \rho_{\text{M}} + \rho_{\text{Pd}}$ for the stable adsorption configurations of *trans*-COOH intermediate over the Pd, Cu@Pd, Au@Pd, Co@Pd, Ni@Pd, Ag@Pd and Al@Pd catalysts. The blue and yellow shaded regions represent the charge loss and charge gain, respectively.

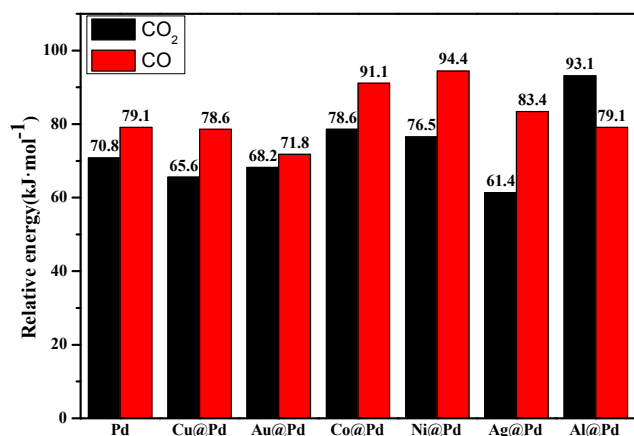


Fig. 10. The reaction energy profile for the rate-determining step in the optimal path of HCOOH dissociation over the Pd, Cu@Pd, Au@Pd, Co@Pd, Ni@Pd, Ag@Pd and Al@Pd catalysts.

formation are 70.8, 65.6, 68.2, 78.6, 76.5, 61.4 and 79.1 kJ·mol⁻¹. It can be seen that the activation barrier of HCOOH dissociation to CO₂ is the highest over the Al@Pd catalyst, which corresponds to the largest

charge transfer. By analyzing the surface Bader charge of Pd atoms, the higher the charge transfer from the subsurface non-noble metal to the surface Pd is, the lower the activity of CO₂ formation in Pd catalyst can be achieved. Namely, an appropriate electron transfer between the shell Pd and the core metal can present better activity toward HCOOH dissociation to CO₂.

Further, a project density of states (pDOS) [66–68] and *d*-band center (ϵ_d) was conducted to explain the catalytic activity over the seven catalysts, the activity order of CO₂ formation is that: Ag@Pd (61.4 kJ·mol⁻¹) > Cu@Pd (65.6 kJ·mol⁻¹) > Au@Pd (68.2 kJ·mol⁻¹) > Pd (70.8 kJ·mol⁻¹) > Ni@Pd (76.5 kJ·mol⁻¹) > Co@Pd (78.6 kJ·mol⁻¹) > Al@Pd (79.1 kJ·mol⁻¹). See Fig. 11, the *d*-band center of the shell Pd over the Pd and M@Pd catalysts show that the ϵ_d of Ag@Pd (-1.67 eV), Cu@Pd (-2.06 eV), Au@Pd (-1.68 eV) and Pd (-1.85 eV) are close the Fermi level, which correspond to better catalytic activity. Whereas the catalytic activity toward HCOOH dissociation to form CO₂ is lower when the ϵ_d of Ni@Pd (-2.57 eV), Co@Pd (-2.76 eV) and Al@Pd (-2.85 eV) are far from the Fermi level.

4. Conclusions

In this study, the mechanism of HCOOH dissociation on the pure Pd and core-shell Cu@Pd, Au@Pd, Co@Pd, Ni@Pd, Ag@Pd, Al@Pd

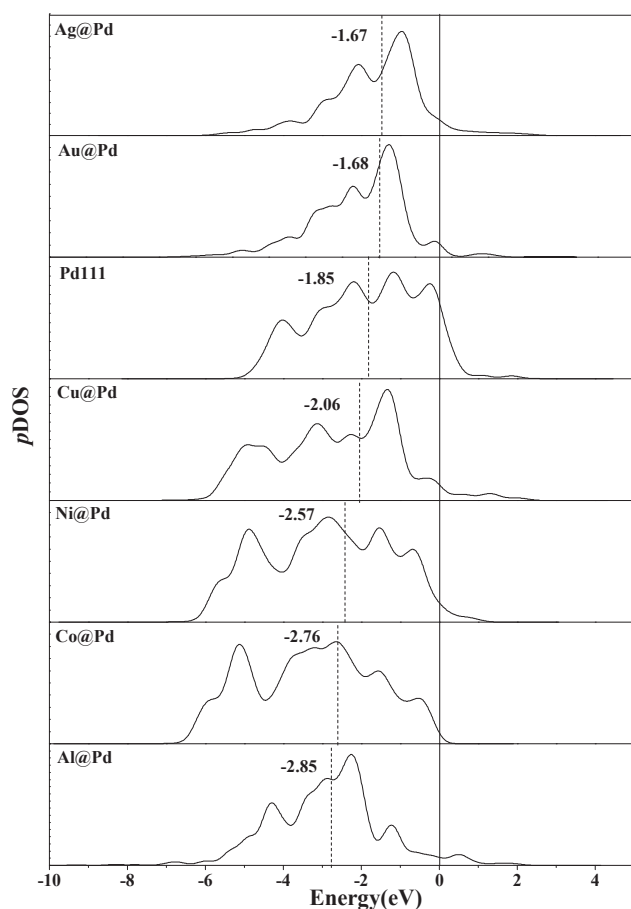


Fig. 11. Partial density of states for the surface Pd atoms of the Ag@Pd, Au@Pd, Pd, Cu@Pd, Ni@Pd, Co@Pd and Al@Pd catalysts. The vertical dashed lines denote the location of the *d*-band center of surface Pd atom. The vertical solid lines represent the Fermi level.

catalysts was systematically studied using DFT calculations and microkinetic modeling. Our results showed that CO is dominantly formed via the COOH intermediate instead of the HCO intermediate; namely, the path via the HCO intermediates can be excluded. However, CO₂ formation mainly goes through the COOH or HCOO intermediate, which depends on the types of core metal. Compared to the pure Pd catalyst, M@Pd (M = Au, Co, Ni, Ag) catalysts are highly selective to the generation of CO₂, while Al@Pd catalyst is favorable for CO formation. Further, the microkinetic modeling result demonstrates that the generation rate of CO₂ on these catalysts at the temperature 298 K is consistent with the results of activation barrier analysis and the calculated selectivity of CO₂ can reach nearly 99.99% over the M@Pd (M = Au, Ag, Ni, Co) catalysts. Among them, the core-shell Ag@Pd catalyst not only presents the best activity and selectivity toward CO₂ generation, but also reduces CO adsorption capacity and enhances the resistance ability toward CO poisoning. Further, for the Ag@Pd catalyst, the non-noble metal Ag incorporation as the core can reduce the usage amount of precious metal Pd, and therefore decrease the cost of the catalyst, which is a potential candidate to enhance the catalytic performance. The results of this study not only help peer scientists clarify the reaction mechanism associated with the corresponding experiments in the field of HCOOH dissociation, but also help them advance the design of cost-effective and structure-tunable M@Pd bimetallic catalysts (materials) with highly catalytic performances needed for HCOOH dissociation, which can have broad impact on catalyst development.

Declaration of Competing Interest

The authors declare that they have no known competing financial interests or personal relationships that could have appeared to influence the work reported in this paper.

Acknowledgment

This work is financially supported by the National Natural Science Foundation of China (No. 21736007 and 21776193), the China Scholarship Council (201606935026) and the Top Young Innovative Talents of Shanxi.

Appendix A. Supplementary material

Supplementary data to this article can be found online at <https://doi.org/10.1016/j.apsusc.2019.144938>.

References

- [1] Y. Yang, H.X. Xu, D.P. Cao, X.C. Zeng, D.J. Cheng, Hydrogen production via efficient formic acid decomposition: engineering the surface structure of Pd-based alloy catalysts by design, *ACS Catal.* 9 (2019) 781–790.
- [2] M. Ojeda, E. Iglesia, Formic acid dehydrogenation on Au based catalysts at near-ambient temperatures, *Angew. Chem. Int. Ed.* 48 (2009) 4800–4803.
- [3] G. Wang, Y. Morikawa, T. Matsumoto, J. Nakamura, Why is formate synthesis insensitive to copper surface structures? *J. Phys. Chem. B* 110 (2006) 9–11.
- [4] J.S. Yoo, F. Abild-Pedersen, J.K. Nørskov, F. Studt, Theoretical analysis of transition-metal catalysts for formic acid decomposition, *ACS Catal.* 4 (2014) 1226–1233.
- [5] A.K. Singh, S. Singh, A. Kumar, Hydrogen energy future with formic acid: a renewable chemical hydrogen storage system, *Catal. Sci. Technol.* 6 (2016) 12–40.
- [6] M. Grasemann, G. Laurency, Formic acid as a hydrogen source—recent developments and future trends, *Energy Environ. Sci.* 5 (2012) 8171–8181.
- [7] N.M. Marković, H.A. Gasteiger, P.N. Ross Jr, X.D. Jiang, I. Villegas, M.J. Weaver, Electro-oxidation mechanisms of methanol and formic acid on Pt-Ru alloy surfaces, *Electrochim. Acta* 40 (1995) 91–98.
- [8] C. Rice, S. Ha, R.I. Masel, P. Waszczuk, A. Wieckowski, T. Barnard, Direct formic acid fuel cells, *J. Power Sources* 111 (2002) 83–89.
- [9] J.B. Xu, T.S. Zhao, Z.X. Liang, Carbon supported platinum-gold alloy catalyst for direct formic acid fuel cells, *J. Power Sources* 185 (2008) 857–861.
- [10] S. Zhang, Y.Y. Shao, G.P. Yin, Y.H. Lin, Facile synthesis of PtAu alloy nanoparticles with high activity for formic acid oxidation, *J. Power Sources* 195 (2010) 1103–1106.
- [11] Z. Jiang, P. Qin, T. Fang, Decomposition mechanism of formic acid on Cu (111) surface: a theoretical study, *Appl. Surf. Sci.* 396 (2017) 857–864.
- [12] J. Cho, S. Lee, S.P. Yoon, J. Han, S.W. Nam, K.-Y. Lee, H.C. Ham, Role of heteronuclear interactions in selective H₂ formation from HCOOH decomposition on bimetallic Pd/M (M = late transition FCC metal) catalysts, *ACS Catal.* 7 (2017) 2553–2562.
- [13] J. Cho, S. Lee, J. Han, S.P. Yoon, S.W. Nam, S.H. Choi, K.-Y. Lee, H.C. Ham, Importance of ligand effect in selective hydrogen formation via formic acid decomposition on the bimetallic Pd/Ag catalyst from first-principles, *J. Phys. Chem. C* 118 (2014) 22553–22560.
- [14] D.A. Bulushev, S. Beloshapkin, J.R.H. Ross, Hydrogen from formic acid decomposition over Pd and Au catalysts, *Catal. Today* 154 (2010) 7–12.
- [15] N. Hoshi, K. Kida, M. Nakamura, M. Nakada, K. Osada, Structural effects of electrochemical oxidation of formic acid on single crystal electrodes of palladium, *J. Phys. Chem. B* 110 (2006) 12480–12484.
- [16] J.Y. Wang, H.X. Zhang, K. Jiang, W.B. Cai, From HCOOH to CO at Pd electrodes: a surface-enhanced infrared spectroscopy study, *J. Am. Chem. Soc.* 133 (2011) 14876–14879.
- [17] J.L. Yu, P.E. Savage, Decomposition of formic acid under hydrothermal conditions, *Ind. Eng. Chem. Res.* 37 (1998) 2–10.
- [18] Z. Liu, X. Zhang, Carbon-supported PdSn nanoparticles as catalysts for formic acid oxidation, *Electrochem. Commun.* 11 (2009) 1667–1670.
- [19] Z.H. Zhang, J.J. Ge, L. Ma, J.H. Liao, T.H. Lu, W. Xing, Highly active carbon-supported PdSn catalysts for formic acid electrooxidation, *Fuel Cells* 9 (2009) 114–120.
- [20] R.S. Li, Z. Wei, T. Huang, A.S. Yu, Ultrasonic-assisted synthesis of Pd-Ni alloy catalysts supported on multi-walled carbon nanotubes for formic acid electro-oxidation, *Electrochim. Acta* 56 (2011) 6860–6865.
- [21] Y.W. Gao, G. Wang, B. Wu, C. Deng, Y. Gao, Highly active carbon-supported PdNi catalyst for formic acid electrooxidation, *J. Appl. Electrochem.* 41 (2011) 1–6.
- [22] L.P. Shen, H.Z. Li, L. Lu, Y.F. Luo, Y.W. Tang, Y. Chen, T.H. Lu, Improvement and mechanism of electrocatalytic performance of Pd-Ni/C anodic catalyst in direct formic acid fuel cell, *Electrochim. Acta* 89 (2013) 497–502.
- [23] Y.Z. Lu, W. Chen, PdAg alloy nanowires: facile one-step synthesis and high electrocatalytic activity for formic acid oxidation, *ACS Catal.* 2 (2012) 84–90.
- [24] K. Mori, M. Dojo, H. Yamashita, Pd and Pd-Ag nanoparticles within a macroreticular basic resin: an efficient catalyst for hydrogen production from formic acid decomposition, *ACS Catal.* 3 (2013) 1114–1119.

- [25] J. Liu, L.X. Lan, R. Li, X.Y. Liu, C. Wu, Agglomerated Ag-Pd catalyst with performance for hydrogen generation from formic acid at room temperature, *Int. J. Hydrogen Energy* 41 (2016) 951–958.
- [26] L. Dai, S.Z. Zou, Enhanced formic acid oxidation on Cu-Pd nanoparticles, *J. Power Sources* 196 (2011) 9369–9372.
- [27] M.J. Ren, Y. Zhou, F.F. Tao, Z.Q. Zou, L. Akins Daniel, H. Yang, Controllable modification of the electronic structure of carbon supported core-shell Cu@Pd Catalysts for formic acid oxidation, *J. Phys. Chem. C* 118 (2014) 12669–12675.
- [28] F. He, K. Li, G.Y. Xie, Y. Wang, M.G. Jiao, H. Tang, Z.J. Wu, Understanding the enhanced catalytic activity of Cu₁@Pd₃(111) in formic acid dissociation, a theoretical perspective, *J. Power Sources* 316 (2016) 8–16.
- [29] X. Wang, Y. Xia, Electrocatalytic performance of PdCo-C catalyst for formic acid oxidation, *Electrochem. Commun.* 10 (2008) 1644–1646.
- [30] B.S. Choi, J. Song, M.J. Song, B.S. Goo, Y.W. Lee, Y. Kim, H. Yang, S.W. Han, Core-shell engineering of Pd-Ag bimetallic catalysts for efficient hydrogen production from formic acid decomposition, *ACS Catal.* 9 (2019) 819–826.
- [31] Y. Huang, X. Zhou, M. Yin, C.P. Liu, W. Xing, Novel PdAu@Au/C core-shell catalyst: superior activity and selectivity in formic acid decomposition for hydrogen generation, *Chem. Mater.* 22 (2010) 5122–5128.
- [32] K. Tedsree, T. Li, S. Jones, C.W.A. Chan, K.M.K. Yu, P.A.J. Bagot, E.A. Marquis, G.D.W. Smith, S.C.E. Tsang, Hydrogen production from formic acid decomposition at room temperature using a Ag-Pd core-shell nanocatalyst, *Nat. Nanotechnol.* 6 (2011) 302–307.
- [33] Z.L. Wang, J.M. Yan, H.L. Wang, Y. Ping, Q. Jiang, Au@Pd core-shell nanoclusters growing on nitrogen-doped mildly reduced graphene oxide with enhanced catalytic performance for hydrogen generation from formic acid, *J. Mater. Chem. A* 1 (2013) 12721–12725.
- [34] O. Metin, X.L. Sun, S.H. Sun, Monodisperse gold-palladium alloy nanoparticles and their composition-controlled catalysis in formic acid dehydrogenation under mild conditions, *Nanoscale* 5 (2013) 910–912.
- [35] K. Mori, T. Sano, H. Kobayashi, H. Yamashita, Surface engineering of a supported PdAg catalyst for hydrogenation of CO₂ to formic acid: elucidating the active Pd atoms in alloy nanoparticles, *J. Am. Chem. Soc.* 140 (2018) 8902–8909.
- [36] G. Kresse, J. Furthmüller, Efficiency of ab-initio total energy calculations for metals and semiconductors using a plane-wave basis set, *Comput. Mater. Sci.* 6 (1996) 15–50.
- [37] G. Kresse, J. Furthmüller, Efficient iterative schemes for ab-initio total-energy calculations using a plane-wave basis set, *Phys. Rev. B* 54 (1996) 11169–11186.
- [38] P. Hohenberg, W. Kohn, Inhomogeneous electron gas, *Phys. Rev.* 136 (1964) B864–B871.
- [39] W. Kohn, L.J. Sham, Self-consistent equations including exchange and correlation effects, *Phys. Rev.* 140 (1965) 1133–1138.
- [40] P.E. Blöchl, Projector augmented-wave method, *Phys. Rev. B: Condens. Matter.* 50 (1994) 17953–17979.
- [41] J.P. Perdew, Y. Wang, Accurate and simple analytic representation of the electron-gas correlation energy, *Phys. Rev. B* 45 (1992) 13244–13249.
- [42] J.P. Perdew, K. Burke, M. Ernzerhof, Generalized gradient approximation made simple, *Phys. Rev. Lett.* 77 (1996) 3865–3868.
- [43] H.J. Monkhorst, J.D. Pack, Special points for brillouin-zone integrations, *Phys. Rev. B: Condens. Matter Mater. Phys.* 13 (1976) 135188–135192.
- [44] D. Sheppard, P.H. Xiao, W. Chemelewski, D.D. Johnsonand, G. Henkelman, A generalized solid-state nudged elastic band method, *J. Phys. Chem.* 136 (2012) 074103–074108.
- [45] D. Sheppard, R. Terrell, G. Henkelman, Optimization methods for finding minimum energy paths, *J. Chem. Phys.* 128 (2008) 385–404.
- [46] G. Henkelman, H. Jónsson, A dimer method for finding saddle points on high dimensional potential surfaces using only first derivatives, *J. Phys. Chem.* 111 (1999) 7010–7022.
- [47] R.A. Olsen, G.J. Kroes, G. Henkelman, A. Arnaldsson, Comparison of methods for finding saddle points without knowledge of the final states, *J. Phys. Chem.* 121 (2004) 9776–9792.
- [48] R.G. Zhang, M. Yang, M. Peng, L.X. Ling, B.J. Wang, Understanding the role of Pd:Cu ratio, surface and electronic structures in Pd-Cu alloy material applied in direct formic acid fuel cells, *Appl. Surf. Sci.* 465 (2019) 730–739.
- [49] Q.Z. Dong, W.X. Zeng, H.S. Wan, S.M. Yu, C.C. Guo, M.L. Huang, Highly effective PdCu electrocatalysts supported on polyelectrolyte functionalized titanium dioxide for direct formic acid fuel cells, *Int. J. Electrochem. Sci.* 12 (2017) 1389–1400.
- [50] K.H. Miao, Y. Luo, J.S. Zou, J. Yang, F.Q. Zhang, L. Huang, J. Huang, X.W. Kang, S.W. Chen, PdRu alloy nanoparticles of solid solution in atomic scale: out-performance towards formic acid electro-oxidation in acidic medium, *Electrochim. Acta* 251 (2017) 588–594.
- [51] Y. Fan, Y. Zhang, H. Li, W. Shen, J. Wang, M. Wei, Three-dimensional highly branched Pd₃Cu alloy multipods as enhanced electrocatalysts for formic acid oxidation, *RSC Adv.* 6 (2016) 43980–43984.
- [52] P. Wang, S.N. Steinmann, G. Fu, C. Michel, P. Sautet, Key role of anionic doping for H₂ production from formic acid on Pd(111), *ACS Catal.* 7 (2017) 1955–1959.
- [53] B. Eren, D. Zherebetsky, L.L. Patera, C.H. Wu, H. Bluhm, C. Africh, L.W. Wang, G.A. Somorjai, M. Salmeron, Activation of Cu(111) surface by decomposition into nanoclusters driven by CO adsorption, *Science* 351 (2016) 475–478.
- [54] K. Brandt, M.E. Chiu, D.J. Watson, M.S. Tikhov, R.M. Lambert, Chemoselective catalytic hydrogenation of acrolein on Ag(111): effect of molecular orientation on reaction selectivity, *J. Am. Chem. Soc.* 131 (2009) 17286–17290.
- [55] W. Luo, A. Asthagiri, Density functional theory study of methanol steam reforming on Co(0001) and Co(111) Surfaces, *J. Phys. Chem. C* 118 (2014) 15274–15285.
- [56] T. Saelee, S. Namuangruk, N. Kungwan, A. Junkaew, Theoretical insight into catalytic propane dehydrogenation on Ni(111), *J. Phys. Chem. C* 122 (2018) 14678–14690.
- [57] L.H. Fan, J.X. Cao, D.O. Physics, The catalytic effect of transition metal doped Al (111) surfaces for hydrogen splitting, *Acta Phys. Sin.* 64 (2015) 038801–038808.
- [58] N.W. Ashcroft, N.D. Mermin, *Solid State Physics*, Saunders College Publishing, 1976.
- [59] D.W. Yuan, Z.R. Liu, Atomic ensemble effects on formic acid oxidation on PdAu electrode studied by first-principles calculations, *J. Power Sources* 224 (2013) 241–249.
- [60] T. Duan, R.G. Zhang, L.X. Ling, B.J. Wang, Insights into the effect of Pt atomic ensemble on HCOOH oxidation over Pt-decorated Au bimetallic catalyst to maximize Pt utilization, *J. Phys. Chem. C* 120 (2016) 2234–2246.
- [61] M.E. Vela, R.O. Lezna, N.R. Detacconi, A.J. Arvia, B. Beden, F. Hahn, C. Lamy, EMIRS studies of formic acid electrooxidation on Pd, Au and Pd+Au alloys: Part 1. Investigation of the adsorbates derived from HCOOH and NACOOH chemisorption at Pd in acid and alkaline solutions, *J. Electroanal. Chem.* 323 (1992) 289–302.
- [62] Y.X. Chen, M. Heinen, Z. Jusys, R.J. Behrn, Bridge-bonded formate: active intermediate or spectator species in formic acid oxidation on a Pt film electrode? *Langmuir* 22 (2006) 10399–10408.
- [63] Y.Y. Qi, R.G. Zhu, D.G. Zhang, Adsorption behaviors of monomer and dimer of formic acid on Pt (111) in the absence and presence of water, *J. Mol. Model.* 20 (2014) 2264–2272.
- [64] S. Singh, S. Li, R. Carrasquillo-Flores, A.C. Alba-Rubio, J.A. Dumesic, M. Mavrikakis, Formic acid decomposition on Au catalysts: DFT, microkinetic modeling, and reaction kinetics experiments, *AIChE J.* 60 (2014) 1303–1319.
- [65] R.G. Zhang, H.Y. Liu, B.J. Wang, L.X. Ling, Insights into the preference of CO₂ formation from HCOOH decomposition on Pd surface: a theoretical study, *J. Phys. Chem. C* 116 (2012) 22266–22280.
- [66] B. Hwang, H. Kwon, J. Ko, B.K. Kim, J.W. Han, Density functional theory study for the enhanced sulfur tolerance of Ni catalysts by surface alloying, *Appl. Surf. Sci.* 429 (2018) 87–94.
- [67] Q. Fu, Y. Luo, Active sites of Pd-doped flat and stepped Cu(111) surfaces for H₂ dissociation in heterogeneous catalytic hydrogenation, *ACS Catal.* 3 (2013) 1245–1252.
- [68] X.R. Cao, Q. Fu, Y. Luo, Catalytic activity of Pd-doped Cu nanoparticles for hydrogenation as a single-atom-alloy catalyst, *Phys. Chem. Chem. Phys.* 16 (2014) 8367–8375.